J Solid State Electrochem (2009) 13:799–805
DOI 10.1007/s10008-008-0757-2

ORIGINAL PAPER

Synthesis and electrochemical properties of nanostructured $LiAl_xMn_{2-x}O_{4-y}Br_y$ particles

Yudai Huang · Rongrong Jiang · Shu-Juan Bao · Zhifang Dong · Yali Cao · Dianzeng Jia · Zaiping Guo

Received: 17 September 2008 / Revised: 13 November 2008 / Accepted: 24 November 2008 / Published online: 6 December 2008

Abstract Nanostructured $LiAl_xMn_{2-x}O_{4-y}Br_y$ particles were synthesized successfully by annealing the mixed precursors, which were prepared by room-temperature solid-state coordination method using lithium acetate, manganese acetate, lithium bromide, aluminum nitrate, citric acid, and polyethylene glycol 400 as starting materials. X-ray diffractometer patterns indicated that the particles of the as-synthesized samples are well-crystallized pure spinel phase. Transmission electron microscopy images showed that the $LiAl_xMn_{2-x}O_{4-y}Br_y$ samples consist of small-sized nanoparticles. The results of galvanostatic cycling tests revealed that the initial discharge capacity of $LiAl_{0.05}Mn_{1.95}O_{3.95}Br_{0.05}$ is 119 mAh g^{-1}; after the 100th cycle, its discharge capacity still remains at 92 mAh g^{-1}. The introduction of Al and Br in $LiMn_2O_4$ bring a synergetic effect and is quite effective in increasing the capacity and elevating cycling performance.

Keywords Nanostructured $LiAl_xMn_{2-x}O_{4-y}Br_y$ particles · Synthesis · Electrochemical properties · Lithium-ion battery

Y. Huang · Y. Cao · D. Jia (✉)
School of Science, Xi'an Jiaotong University,
Xi'an 710049, People's Republic of China
e-mail: jdz@xju.edu.cn

Y. Huang · R. Jiang · S.-J. Bao · Z. Dong · Y. Cao · D. Jia · Z. Guo
Institute of Applied Chemistry, Xinjiang University,
Urumqi 830046, People's Republic of China

Z. Guo
Institute for Superconducting and Electronic Materials,
University of Wollongong,
Wollongong, NSW 2522, Australia

Introduction

Lithium-ion or "rocking-chair" batteries are the state of art advanced batteries due to its high potential, elevated energy density, long shelf-life, and safety. Layered $LiCoO_2$ is currently used as positive electrode in commercial lithium-ion batteries; however, it suffers from the high cost and biotoxicity of cobalt. Consequently, it is of importance to search for alternatives, and the most promising materials are identified as $LiNiO_2$, $LiMn_2O_4$, and their related derivatives. Intensive research has particularly focused on $LiMn_2O_4$ because of the low cost and nontoxicity of manganese. Despite such merits, $LiMn_2O_4$ still has difficulty in practical applications, owing to its severe capacity depletion. To overcome this problem, many researchers have studied the mechanism of capacity fading and many methods for the cyclability improvement of spinel cathodes have been suggested [1–3].

Doping [4–5] is considered to be an effective path to improve the electrochemical performance of $LiMn_2O_4$, so several attempts have been made for improved synthesis of lithium manganese spinels by doping with various metals, such as Al, Mg, Co, Cr, etc. [6–9]. Although such substitutions often result in enhancing the stability of spinel, the initial discharge capacity of the dope-typed spinels decreases significantly and lower than that of the parent compound. The reduction in capacity is mainly due to the fact that the substituent ions do not contribute to the charge capacity. In 1999, Amatucci et al. [10] and Palacin et al. [11] reported that fluorine doping at the oxygen site is quite effective for improving the battery performance of $LiMn_2O_4$ and increasing the initial capacity. Jiang et al. [12] reported that Li and F codoped spinels show better

synergetic effect and not only increased the capacity but also elevated the cycling performance of battery. Wu et al. [13] prepared $LiAl_yMn_{2-y}O_{4-z}F_z$ cathode materials, and found that they have better cycling performance than $LiMn_2O_4$. Sun et al. [14–15] also reported that Al and S codoped materials prepared via a sol–gel method which showed excellent cyclability in both 4 and 3 V regions. Therefore, cation and anion cosubstitutions can be assumed to an alternate way of improving the materials' electrochemical properties. Up to now, no Al and Br codoped spinels were reported.

Another factor affecting the electrochemical behavior, especially the capacity, is dependent on the microstructure of the resulting compounds. It is reported that nanomaterials show higher capacity and better cycling performance than conventional electrodes which are composed of the same materials. For instance, Myung et al. synthesized nanosized $LiMnO_2$ via hydrothermal reaction at 170 °C. The results of the charge–discharge experiment showed a better discharge capacity and longer cycle stability [16]. So there have been increased interests in synthesizing nanostructured compounds and applying them in lithium-ion batteries, such as nanorods, nanowires, nanotubes, nanobelts, and nanoribbons. Moreover, it is well-known that the preparation methods and post-treatment techniques have significant influences on the microstructure and particle size distribution of the products. These physical characteristics of electrodes materials will further affect their electrochemical properties, such as discharge capacity, discharge rate, reversibility, and cyclability [17]. Room-temperature solid-state coordination method is a simple and effective method to fabricate a number of chemical compounds. Cluster compounds, coordination compounds, solid coordination compounds, etc. have been synthesized by this method in the past years in our research group. This method possesses the advantages of simple manipulation, high efficiency, low energy consumption, convenient operation, and low pollution [18, 19]. More meaningfully, it achieves homogeneous mixing of the starting components and it is easy to obtain small grain-sized particles [20].

In this work, nanostructured $LiMn_2O_4$ particles doped with Br and Al were synthesized by a room-temperature solid-state coordination method. The structure, morphology, and electrochemical properties of the products were also investigated in detail.

Experimental

Preparation

$LiAl_xMn_{2-x}O_{4-y}Br_y$ (x=0, 0.05, 0.10, 0.15; y=0, 0.05, 0.1) compounds were synthesized by annealing the mixed precursors, which were prepared by a room-temperature solid-state coordination method with lithium acetate, manganese acetate, lithium bromide, aluminum nitrate, and citric acid (worked as chelating reagent, molar ratio of citric acid to the total metal ions is 1:1) as starting materials. Briefly, raw materials at a molar ratio of Li/Al/Mn/Br/citric acid of 1-y:x:2-x:y:3 were mixed with polyethylene glycol (PEG) 400 (worked as dispersants) in an agate mortar and ground for 1 h, and then the mixture was heated at 120 °C in vacuum oven for 8 h to form precursors. The obtained precursors were annealed at 500 °C for 1 h, ground, and annealed at 700 °C for 10 h in a muffle furnace in air to obtain the final $LiAl_xMn_{2-x}O_{4-y}Br_y$ particles.

Characterization

Powder X-ray diffractometer (XRD; MXP18AHF, MAC, Japan) using Cu Kα radiation (λ=1.54056 Å) was used for the identification of the crystalline phases of the particles. Rietveld refinement by using the FULLPROF program was then performed on the XRD data to obtain lattice constants. The grain size and morphology of the samples were observed using transmission electron microscopy (TEM; H-600, Hitachi, Japan). The average particle size was calculated using the Scherrer formula (d_{111}) and listed in Table 1 for all of the samples.

Electrochemical measurements

The cells consisted of a $LiMn_2O_4$-based composite as the positive electrode, a Li disk as the negative electrode, and an electrolyte of 1 M $LiPF_6$ in a 1:1 (volume ratio) mixture of ethylene carbonate/dimethyl carbonate. The cathode was formed by mixing the active material with acetylene black and polyvinylidene fluoride binder in a 85:10:5 ratio in *N*-methyl-pyrrolidone, which acts as the solvent for the binder. The paste was applied to Al foil current collectors using a blade. The film was dried at 60 °C in air for 1 h and then was vacuum-dried at 120 °C for 4 h. The weight of the electrochemical active material was calculated from the total weight of the electrodes and the weight of the Al foil

Table 1 Lattice constants and crystallite size measured by Rietveld analysis and Scherrer formula (d_{111})

Nominal composition	Lattice constant, a (nm)	Crystallite size (nm)
$LiMn_2O_4$	0.823415	26
$LiMn_2O_{3.95}Br_{0.05}$	0.825630	27
$LiMn_2O_{3.90}Br_{0.10}$	0.825765	35
$LiAl_{0.05}Mn_{1.95}O_{3.95}Br_{0.05}$	0.822828	55
$LiAl_{0.10}Mn_{1.90}O_{3.95}Br_{0.05}$	0.821403	28
$LiAl_{0.15}Mn_{1.85}O_{3.95}Br_{0.05}$	0.820941	36

and additives. Celgard 2300 membrane was used as the separator. The cells were assembled in an argon-filled glove box. All the electrochemical tests were carried out at room temperature. Cyclic voltammetry (CHI660B electrochemical workstation; Chenhua, Shanghai, China) experiments were conducted at a scan rate of 0.1 mV s^{-1}, and a Li metal disk served as both counter and reference electrode. Charge/discharge tests were performed at a constant current density of 0.30 mA cm^{-2} (0.5C) within the potential range of 3.0 and 4.35 V.

Results and discussion

The crystal structures of $LiAl_xMn_{2-x}O_{4-y}Br_y$ particles were characterized by XRD. All of the samples were synthesized under the same preparation conditions as described in the "Experimental" section by changing the stoichiometric compositions of the corresponding starting materials. The diffraction peaks of all of the samples are displayed in Fig. 1, which corresponded to pure-phase spinel structure. The results indicated that the structure of the ternary spinel remained while some of the O in the spinel phase was replaced by Br and Mn by Al. The doping did not seem to change the spinel structures since no impurity peaks were observed in the XRD patterns. The lattice constants of all of the samples were listed in Table 1, which were calculated via the Rietveld refinement by using the FULLPROF program from the XRD data of Fig. 1. The lattice constants linearly increased from 0.823415 Å for the undoped $LiMn_2O_4$, 0.825630 Å for $LiMn_2O_{3.95}Br_{0.05}$ to 0.825765 Å for $LiMn_2O_{3.90}Br_{0.10}$. The products doped with Br ions have larger lattice constant, which is ascribed to the substitution of the oxygen ion by Br ion. The ion radius of Br ion (1.96 Å) is larger than that of oxygen ion (1.4 Å) and Br substitution will lead to the reduction of part of Mn^{4+} to larger Mn^{3+} cations, which result in the increase of samples' lattice constant. Differently, substitution of manganese with aluminum results in shrinkage of the unit cell volume [9]. The lattice constants of $LiAl_{0.05}Mn_{1.95}O_{3.95}Br_{0.05}$, $LiAl_{0.10}Mn_{1.90}O_{3.95}Br_{0.05}$, and $LiAl_{0.15}Mn_{1.85}O_{3.95}Br_{0.05}$ are 0.822828, 0.821403, and 0.820941 Å, respectively, which results in the stability of the spinel structure and decreases the capacity loss of the $Li/LiAl_xMn_{2-x}O_4$ cells after many cycles. Compared with $LiMn_2O_{4-y}Br_y$, the lattice constants decreased gradually with the increase of Al substitution amount. This is because the Al ion has smaller ionic radius than manganese ion: Al^{3+} (0.53 Å), Mn^{3+} (0.66 Å), Mn^{4+} (0.60 Å) [10]. In addition, the bonding energy of the Al–O bond (1,298 kJ/moL) is stronger than that of Mn–O bond (946 kJ/moL).

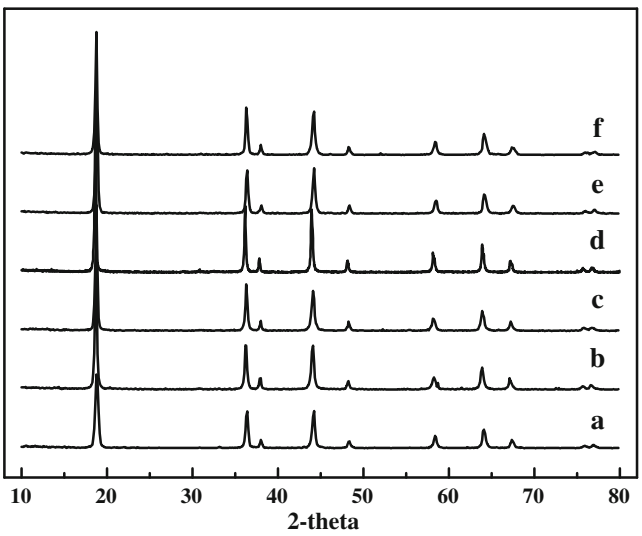

Fig. 1 XRD patterns of $LiAl_xMn_{2-x}O_{4-y}Br_y$: **a** $LiMn_2O_4$; **b** $LiMn_2O_{3.95}Br_{0.05}$; **c** $LiMn_2O_{3.90}Br_{0.10}$; **d** $LiAl_{0.05}Mn_{1.95}O_{3.95}Br_{0.05}$; **e** $LiAl_{0.10}Mn_{1.90}O_{3.95}Br_{0.05}$; **f** $LiAl_{0.15}Mn_{1.85}O_{3.95}Br_{0.05}$

According to literature report [10], the increase of Mn^{3+} will elevate the initial specific capacity. However, Mn^{3+} was the original reason for the Jahn–Teller distortion, which causes the capacity fading. But, considering the effect of increasing capacity of Br ion dopant, which can probably compensate the defect of cation substitution, the anion and cation cosubstitution does provide a new useful way in improving the structural/chemical aspects of the spinel $LiMn_2O_4$.

The TEM images of $LiAl_xMn_{2-x}O_{4-y}Br_y$ particles are exhibited in Fig. 2. It is found that the as-prepared samples have similar morphology with uniform size distribution. The average particle sizes of the samples by calculating using the Scherrer formula are listed in Table 1. As can be seen from Table 1, the particle size for all of the samples is smaller than 60 nm. The calculated value is a little smaller than that observed from TEM images, which indicated that, during the preparation process, the samples agglomerated to a certain extent. It is well-known that the smaller particle size of electrode materials will result in increasing liquid–solid interfacial area and facilitated electrolyte diffusion. Consequently, reduction of the particle size might be favorable for the insertion and extraction of lithium ion from the lithium-ion battery electrode materials [21]; hence, this may improve the electrochemical properties of the as-prepared samples.

Figure 3 displays the voltage versus discharge capacity curves for $LiMn_2O_{4-y}Br_y$ ranging from 3 to 4.35 V versus Li/Li^+ by applying a current density of 0.3 mA cm^{-2} (0.5C) at room temperature. As can be seen from Fig. 3, the initial discharge capacity of pure spinel is 106 mAh g^{-1}. Compared with pure spinel $LiMn_2O_4$, the initial capacity of Br-substituted $LiMn_2O_4$ increases with the increase of Br amount (127 mAh g^{-1} as y=0.05, 118 mAh g^{-1} as y=0.10). This could be explained by the following reason. Substitu-

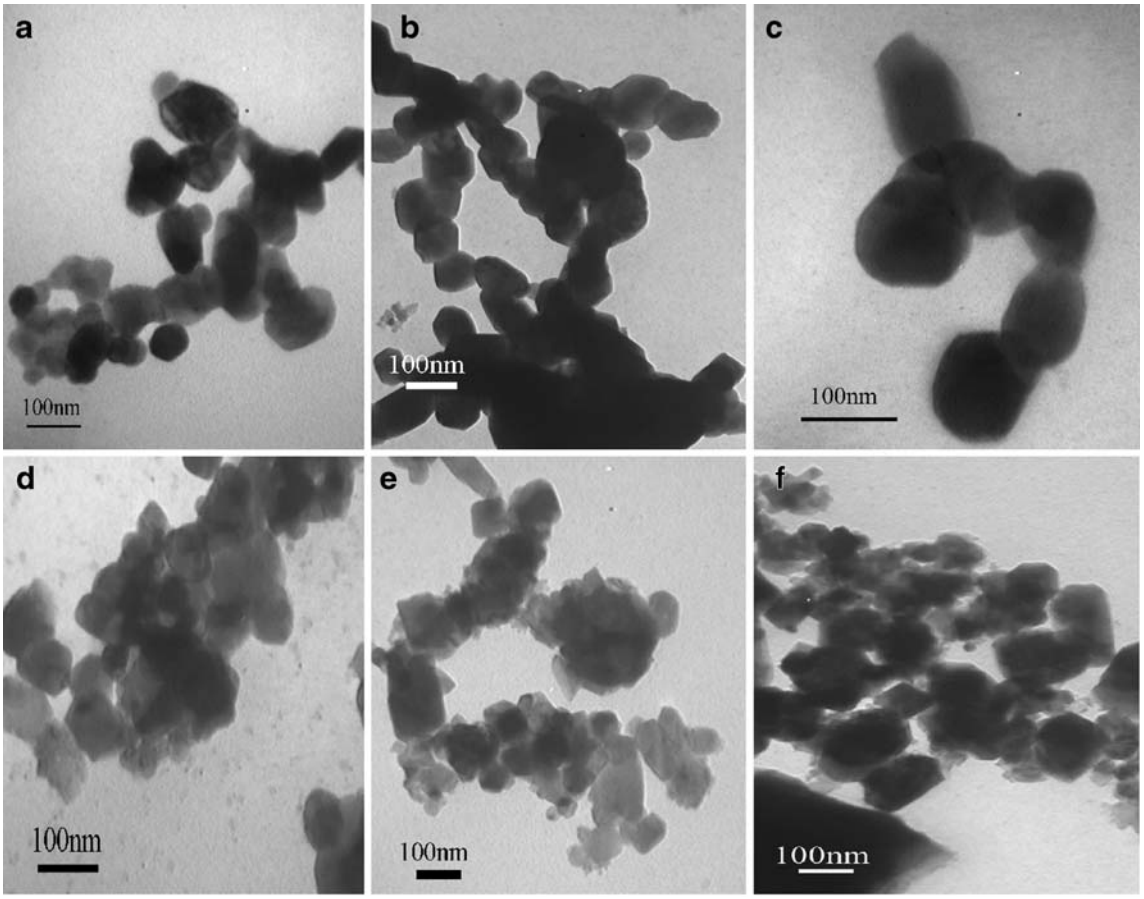

Fig. 2 TEM photographs of $LiAl_xMn_{2-x}O_{4-y}Br_y$: **a** $LiMn_2O_4$; **b** $LiMn_2O_{3.95}Br_{0.05}$; **c** $LiMn_2O_{3.90}Br_{0.10}$; **d** $LiAl_{0.05}Mn_{1.95}O_{3.95}Br_{0.05}$; **e** $LiAl_{0.10}Mn_{1.90}O_{3.95}Br_{0.05}$; **f** $LiAl_{0.15}Mn_{1.85}O_{3.95}Br_{0.05}$

tion of monovalent bromine for divalent oxygen results in the increase of the ratio of Mn^{3+}/Mn^{4+} in samples, and Mn^{3+} contributes to the charge–discharge capacity during insertion/extraction of Li^+ in $LiMn_2O_4$. However, with the increase of Br content (from 0.05 to 0.10), the initial discharge capacity of the samples decreases (from 127 to 118 mAh g^{-1}). When the content of Br increases to 0.05, its initial discharge capacity reaches the highest value, which indicated that the content of Br in spinel $LiMn_2O_4$ has an optimal value; in this work, the optimal value is 0.05.

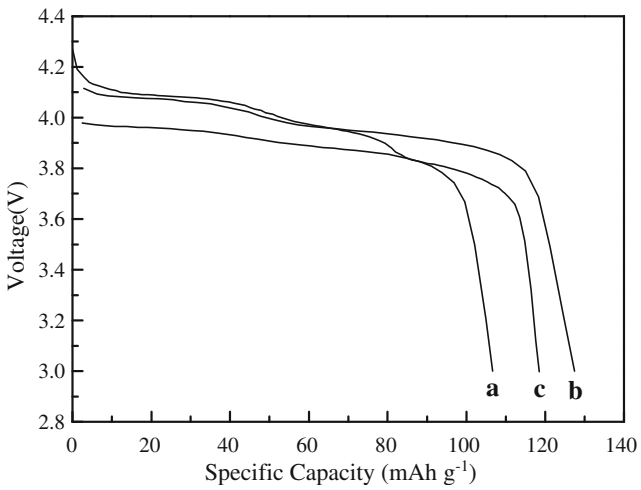

Fig. 3 Voltage versus discharge capacity curves for $LiMn_2O_{4-y}Br_y$: **a** $LiMn_2O_4$; **b** $LiMn_2O_{3.95}Br_{0.05}$; **c** $LiMn_2O_{3.90}Br_{0.10}$

Figure 4 displays the discharge capacity versus cycle number curves of $LiMn_2O_{4-y}Br_y$. Clearly, the samples doped by Br ion have larger initial discharge capacity than the pure spinels. However, Br-doped samples present slight capacity loss after long cycles. The capacity retention rates after 100 cycles for $LiMn_2O_4$, $LiMn_2O_{3.95}Br_{0.05}$, and $LiMn_2O_{3.90}Br_{0.10}$ are 81.8%, 71.4%, and 77.3%, respectively. This is due to monovalent bromine substitution for divalent oxygen that results in the increase of the content of Mn^{3+} in the samples; the high-spin Mn^{3+} gives rise to the Jahn–Teller distortion, which is the origin of the capacity loss. In other words, the increase of the content of Mn^{3+} causes two effects: (1) the increase of initial capacity and (2) the decrease of the capacity retention rates [22]. The capacity retention rate of $LiMn_2O_{3.90}Br_{0.10}$ is higher than that of $LiMn_2O_{3.95}Br_{0.05}$. The reason may be attributed to when the content of Br^- (the Br ion has larger ion radius [1.96 Å] than the O ion [1.4 Å]) increases in the spinel

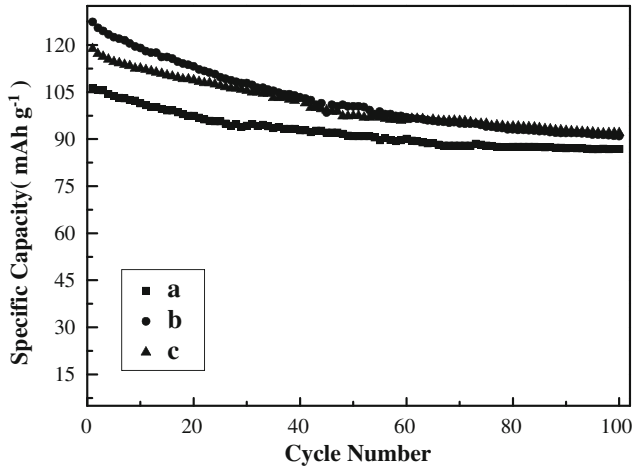

Fig. 4 Discharge capacity versus cycle number curves of $LiMn_2O_{4-y}Br_y$: **a** $LiMn_2O_4$; **b** $LiMn_2O_{3.95}Br_{0.05}$; **c** $LiMn_2O_{3.90}Br_{0.10}$

lattice, the path of insertion and extraction of Li^+ become broader and lead to Li^+ insertion/extraction from the spinel structure become easier.

It has been reported that Al substitution can improve the cycling performance of $LiMn_2O_4$. This is because the bond energy of the Al–O bond (1,298 kJ/moL) is bigger than that of the Mn–O bond (946 kJ/moL) in the octahedron, the total bond energy of metal–oxygen bonds in the Al-doped spinel is bigger than that in the pure spinel, and the strong bond energy increases the stability of the spinel structure of $LiMn_2O_4$. Figure 5 displays the voltage versus discharge capacity curves for $LiAl_xMn_{1.95}O_{3.95}Br_{0.05}$ at a current density of 0.3 mA cm^{-2} (0.5C) at room temperature. The $Li/LiAl_xMn_{2-x}O_{4-y}Br_y$ cells were cycled 100 times, and its cycle characteristics were displayed in Fig. 6. The $LiAl_xMn_{2-x}O_{3.95}Br_{0.05}$ exhibited a lower initial discharge capacity compared with the $LiMn_2O_{3.95}Br_{0.05}$. $LiAl_{0.05}Mn_{1.95}O_{3.95}Br_{0.05}$, $LiAl_{0.10}Mn_{1.90}O_{3.95}Br_{0.05}$, and $LiAl_{0.15}Mn_{1.85}O_{3.95}Br_{0.05}$ delivered the initial discharge capacity of 119, 112, and 104 mAh g^{-1}, respectively. After 100 cycles, their discharge capacity is 92, 88, and 89 mAh g^{-1}, respectively. As expected, the Al and Br codoped in $LiMn_2O_4$ bring a synergetic effect and enhance the discharge capacity and cycle life of the samples. As can be seen from Fig. 6, the initial discharge capacities of these particles decrease with the increase of Al substitution amount in the active materials, which is due to Al substitution decreasing the amount of extractable Li^+ in the spinel. The capacity retention rates of the samples improve gradually with the increase of Al content. After 100 cycles, the discharge capacity retention rates are 77.4%, 78.5%, and 85.5% for $LiAl_{0.05}Mn_{1.95}O_{3.95}Br_{0.05}$, $LiAl_{0.10}Mn_{1.90}O_{3.95}Br_{0.05}$, and $LiAl_{0.15}Mn_{1.85}O_{3.95}Br_{0.05}$, respectively.

The Al and Br codoping in $LiMn_2O_4$ bring a synergetic effect. In this work, the $LiAl_{0.05}Mn_{1.95}O_{3.95}Br_{0.05}$ possesses the best electrochemistry performance, the initial discharge capacity is 119 mAh g^{-1}, and the discharge capacity is 92 mAh g^{-1} after 100 cycles. Hence, further characterization focus on $LiAl_{0.05}Mn_{1.95}O_{3.95}Br_{0.05}$.

Figure 7 shows the charge capacity, discharge capacity, and Coulombic efficiency of $LiAl_{0.05}Mn_{1.95}O_{3.95}Br_{0.05}$. As can be seen from Fig. 7, the capacity loss of $LiAl_{0.05}Mn_{1.95}O_{3.95}Br_{0.05}$ from the first to 100th cycles is very small. The Coulombic efficiency (calculated from the discharge capacity/charge capacity) stays at about 100% except the first cycle. It is well-known that coulombic

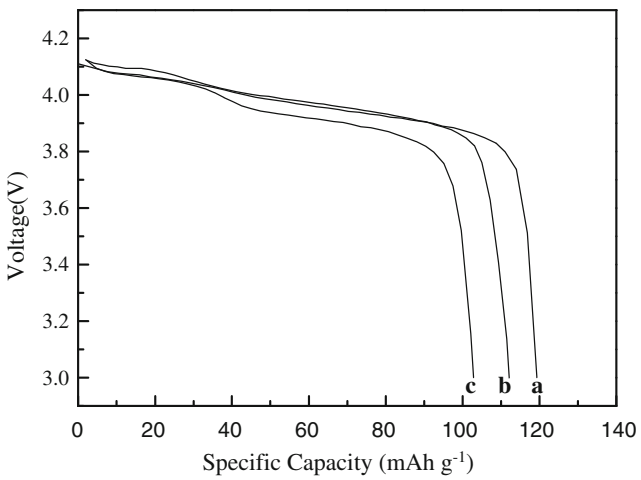

Fig. 5 Voltage versus discharge capacity curves for $LiAl_xMn_{2-x}O_{3.95}Br_{0.05}$: **a** $LiAl_{0.05}Mn_{1.95}O_{3.95}Br_{0.05}$; **b** $LiAl_{0.10}Mn_{1.90}O_{3.95}Br_{0.05}$; **c** $LiAl_{0.15}Mn_{1.85}O_{3.95}Br_{0.05}$

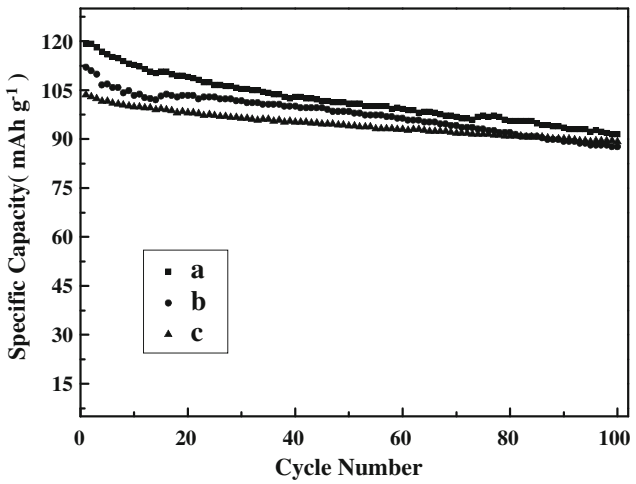

Fig. 6 Discharge capacity versus cycle number curves of $LiAl_xMn_{2-x}O_{3.95}Br_{0.05}$: **a** $LiAl_{0.05}Mn_{1.95}O_{3.95}Br_{0.05}$; **b** $LiAl_{0.10}Mn_{1.90}O_{3.95}Br_{0.05}$; **c** $LiAl_{0.15}Mn_{1.85}O_{3.95}Br_{0.05}$

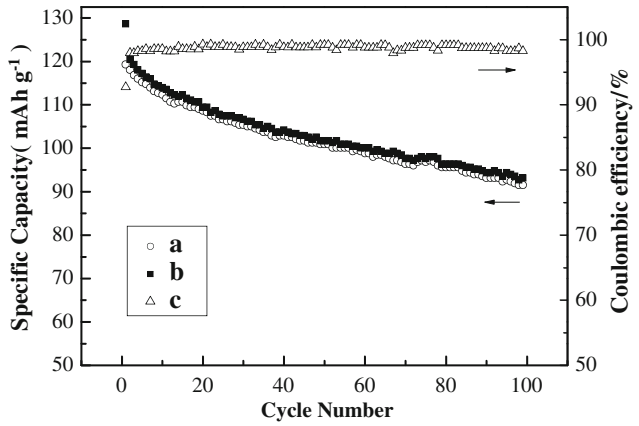

Fig. 7 The charge capacity, discharge capacity, and coulombic efficiency of $LiAl_{0.05}Mn_{1.95}O_{3.95}Br_{0.05}$: **a** discharge capacity; **b** charge capacity; **c** coulombic efficiency

efficiency is an important index in assessing the quality of the lithium-ion battery. Therefore, the results obtained above further confirm that the sample obtained by room-temperature solid-state coordination method is a good candidate for lithium-ion battery cathode materials.

Rate capacity test illustrates more interesting results. As observed in Fig. 8, the discharge capacity of the $Li/LiAl_{0.05}Mn_{1.95}O_{3.95}Br_{0.05}$ cell slowly decreased with increasing current densities and was determined to be 111, 106, and 99 mAh g^{-1} at current densities of 1C, 1.5C, and 2C, respectively. Furthermore, the $Li/LiAl_{0.05}Mn_{1.95}O_{3.95}Br_{0.05}$ cell presented excellent capacity retention at various current densities.

For comparing the electrochemical properties of $LiAl_xMn_{2-x}O_{4-y}Br_y$ and $LiMn_2O_4$, the cyclic voltammograms (CVs) measurements should be also carried out. The CVs of the samples $LiMn_2O_4$ and $LiAl_{0.05}Mn_{1.95}O_{3.95}Br_{0.05}$ before and after 100 cycles at a scan rate of 0.1mV s^{-1}

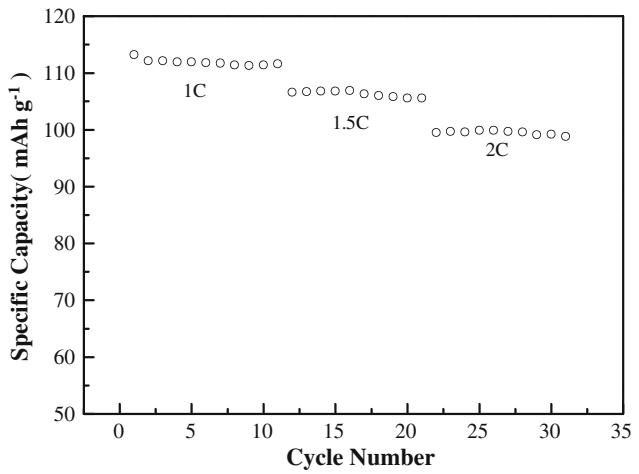

Fig. 8 Discharge capacity versus cycle number curves for the $Li/LiAl_{0.05}Mn_{1.95}O_{3.95}Br_{0.05}$ cell at various current densities

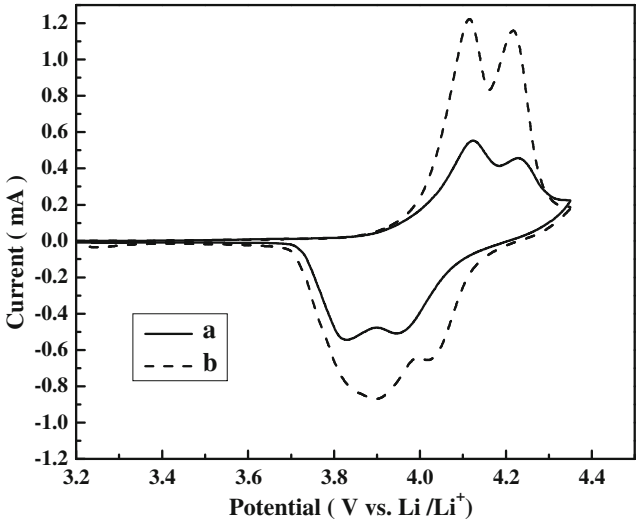

Fig. 9 Cyclic voltammograms of $LiMn_2O_4$ and $LiAl_{0.05}Mn_{1.95}O_{3.95}Br_{0.05}$ before being cycled: **a** $LiMn_2O_4$; **b** $LiAl_{0.05}Mn_{1.95}O_{3.95}Br_{0.05}$

are displayed in Figs. 9 and 10, respectively. As can be seen from Fig. 9, two pairs of peaks are clearly observed in both anode and cathode scans, which are the characteristic of $LiMn_2O_4$ [23]. The peak current of $LiAl_{0.05}Mn_{1.95}O_{3.95}Br_{0.05}$ is higher than that of $LiMn_2O_4$ and the peak potential difference between the two pairs of redox peaks of $LiAl_{0.05}Mn_{1.95}O_{3.95}Br_{0.05}$ is smaller than that of $LiMn_2O_4$, which indicates that $LiAl_{0.05}Mn_{1.95}O_{3.95}Br_{0.05}$ has better electrochemical activity and reversibility than $LiMn_2O_4$. Figure 10 shows the CVs of $LiMn_2O_4$ and $LiAl_{0.05}Mn_{1.95}O_{3.95}Br_{0.05}$ after 100 cycles, the shape of the CVs of pure $LiMn_2O_4$ became poor and two pairs of redox peaks merge to one peak and shift clearly. However, for $LiAl_{0.05}Mn_{1.95}O_{3.95}Br_{0.05}$, after 100 cycles, two pairs of

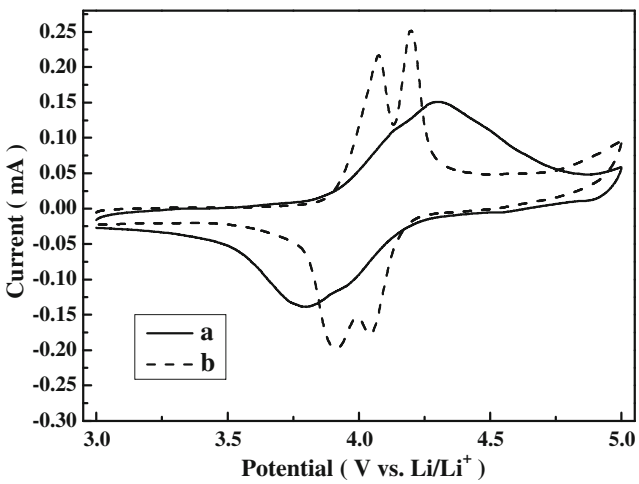

Fig. 10 Cyclic voltammograms of $LiMn_2O_4$ and $LiAl_{0.05}Mn_{1.95}O_{3.95}Br_{0.05}$ after being cycled for 100 cycles: **a** $LiMn_2O_4$; **b** $LiAl_{0.05}Mn_{1.95}O_{3.95}Br_{0.05}$

peaks still clearly separate and correspond to two-step reversible intercalation/deintercalation reaction. This results indicate that the improved structure of the cathode material by Br and Al codoping presents higher reversibility and better capacity retention during cycling. As a result, it is reasonable to choose Br and Al as codopants to elevate the electrochemical properties of $LiMn_2O_4$.

Conclusion

Nanostructured $LiAl_xMn_{2-x}O_{4-y}Br_y$ particles were synthesized for the first time by annealing the mixed precursors, which were prepared by a room-temperature solid-state coordination method. The particles have homogeneous morphology, high crystallinity, and uniform nanosized distribution. The electrochemical test indicated that Br and Al codoping could bring a synergetic effect, improve the initial discharge capacity and the cycle life of spinel $LiMn_2O_4$.

Acknowledgements This work was supported by the Nature Science Foundation of Xinjiang Province (Nos. 200821121 and 200721102) and the National Natural Science Foundation of China (Nos. 20666005 and 20661003).

References

1. Sun YK (1997) Solid State Ion 100:115, doi:10.1016/S0167-2738(97)00311-1
2. Robertson AD, Lu SH, Averill WF, Howard WF Jr (1997) J Electrochem Soc 144:3500, doi:10.1149/1.1838040
3. Amatucci GG, Tarascon JM (1997) US Patent No. 5,674,645
4. Wu YP, Rahm E, Holze R (2002) Electrochim Acta 47:3491, doi:10.1016/S0013-4686(02)00317-1
5. Amatucci GG, Pasquier AD, Blyr A, Zheng T, Tarascon JM (1999) Electrochim Acta 45:255, doi:10.1016/S0013-4686(99)00209-1
6. Komaba S, Oikawa K, Myung ST, Kumagai N, Kamiyama T (2002) Solid State Ion 149:47, doi:10.1016/S0167-2738(02)00168-6
7. Huang YD, Li J, Jia DZ (2005) J Colloid Interface Sci 286:263, doi:10.1016/j.jcis.2004.12.049
8. Yoshio M, Xia Y, Kumada N, Ma S (2001) J Power Sources 101:79, doi:10.1016/S0378-7753(01)00546-8
9. Lee JH, Hong JK, Jang DH, Sun YK, Oh SM (2000) J Power Sources 89:7, doi:10.1016/S0378-7753(00)00375-X
10. Amatucci GG, Pereira N, Zhang T, Plitz I, Tarascon JM (1999) J Power Sources 81–82:39, doi:10.1016/S0378-7753(99)00186-X
11. Palacin MR, Cras FL, Seguin L, Anne M, Chabre Y, Tarascon JM, Amatucci G, Vaughan G, Strobel P (1999) J Solid State Chem 144:361, doi:10.1006/jssc.1999.8166
12. Jiang R, Huang Y, Jia D, Wang L (2007) J Electrochem Soc 154:A698, doi:10.1149/1.2734800
13. Wu X, Zong X, Yang Q, Jin Z, Wu H (2001) J Fluorine Chem 107:39, doi:10.1016/S0022-1139(00)00344-4
14. Sun YK, Jeon YS (1999) J Mater Chem 9:3147, doi:10.1039/a906811b
15. Sun YK (2000) Electrochem Commun 2:6, doi:10.1016/S1388-2481(99)00136-8
16. Myung ST, Komaba S, Kumagai N (2002) Electrochim Acta 47:299
17. Dobley A, Ngala K, Yang S, Zavalij PY, Whittingham MS (2001) Chem Mater 13:4382, doi:10.1021/cm010518h
18. Ye XR, Jia DZ, Yu JQ, Xin XQ, Xue ZL (1999) Adv Mater 11:941, doi:10.1002/(SICI)1521-4095(199908)11:11<941::AID-ADMA941>3.0.CO;2-T
19. Wang RY, Jia DZ, Zhang L, Liu L, Guo ZP, Li BQ, Wang JX (2006) Adv Funct Mater 16:687, doi:10.1002/adfm.200500549
20. Jia DZ, Yu JQ, Xia X (1998) Chin Sci Bull 43:571, doi:10.1007/BF02883641
21. Lu CH, Lin SW (2001) J Power Sources 97–98:458, doi:10.1016/S0378-7753(01)00637-1
22. Capsoni D, Bini M, Chiodelli G, Mustarelli P, Massarotti V, Azzoni CB, Mozzati MC, Linati L (2002) J Phys Chem B 106:7432, doi:10.1021/jp020220u
23. Fujiyoshi H, Waki S (1997) J Power Sources 68:139, doi:10.1016/S0378-7753(96)02623-7